Title: Copper signaling promotes proteostasis and animal development via allosteric activation of ubiquitin E2D conjugases

Authors: C.M. Opazo[1†], A. Lotan[1†], Z. Xiao[1,2†], B. Zhang[3], M.A. Greenough[1], C.M. Lim[4], H. Trytell[1], A. Ramírez[1], A.A. Ukuwela[2], C.H. Mawal[1], J. McKenna[5], D.N. Saunders[5], R. Burke[3], P.R. Gooley[6], A.I. Bush[1†*]

Affiliations: [1]Melbourne Dementia Research Centre, Florey Institute of Neuroscience and Mental Health, The University of Melbourne, Victoria 3010, Australia.

[2]School of Chemistry and Bio21 Molecular Science and Biotechnology Institute, The University of Melbourne, Victoria 3010, Australia.

[3]School of Biological Sciences, Monash University, Wellington Rd, Clayton 3800, Victoria, Australia.

[4]School of Life and Environmental Sciences, Deakin University, Burwood, Melbourne, Victoria 3125, Australia.

[5]School of Medical Sciences, UNSW, Australia.

[6]Department of Biochemistry and Molecular Biology, Bio21 Molecular Science and Biotechnology Institute, University of Melbourne, Parkville, Victoria 3010, Australia

[†]These authors contributed equally to this work.

*Correspondence to: Professor Ashley I. Bush, Melbourne Dementia Research Centre, The Florey Institute of Neuroscience & Mental Health, The University of Melbourne, Victoria 3010, Australia. Tel.: +61 (3) 9035 6532; E-mail: ashley.bush@florey.edu.au

One Sentence Summary: Conserved allostery of ubiquitin E2D conjugases links sub-fM copper signaling to protein degradation and animal morphogenesis.

Summary: Fine-tunning of ubiquitin-conjugating enzymes (E2s), which orchestrate posttranslational modifications that control protein and cell fate, remains largely elusive. Recently, copper signaling emerged as a critical regulator of cell growth and neuronal differentiation, yet confluence of these key pathways has not been reported. Here we show that subtle rises in cellular copper strikingly increase polyubiquitination in numerous mammalian cell lines, while markedly accelerating protein degradation. Using biochemistry, proteomics, NMR spectroscopy and mutational analyses, we link Cu^{+}-enhanced protein ubiquitination and degradation to an evolutionarily conserved CXXXC motif in the E2D (UBE2D) clade. Cu^{+} binding to this sub-femtomolar-affinity site induces allosteric changes that transduce to the active site region and increase enzyme activity. This machinery couples physiologic fluctuations in cytoplasmic Cu^{+} with the degradation rate of numerous proteins including the canonical substrate, p53. In *Drosophila* harboring a larval-lethal UbcD1 knockdown, human E2D2 expression supported near-normal development but ablation of its Cu^{+} binding site profoundly disrupted head development. Our findings introduce Cu^{+} as a novel regulator of E2D activity through an allosteric switch whose emergence coincided with animal multicellularity. Through this unexpected signaling mechanism, crosstalk between copper and protein ubiquitination could have broad impact including upon neurobiological development and cell cycling.

Main Text:

The ubiquitin-conjugating enzymes (E2s) are increasingly appreciated as critical players in the orchestration of ubiquitination, but the functional characterization of sequence diversity within the family, which in humans includes 40 human protein members, is rudimentary(*1, 2*). E2s can be regulated by non-covalent interactions and covalent post-translational modifications, yet the

functional significance of this complex regulation is still notional(*3*). Copper is an indispensable transition metal in animals and has classically been appreciated for its essential structural and catalytic functions(*4*). Novel roles for Cu^+ in cell signaling have recently emerged, where dynamic changes in Cu^+ pools, buffered to the sub-femtomolar (fM) range by abundant glutathione (GSH)(*5*), modulate protein function and cell physiology(*6*). GSH also maintains active site sulfhydryl residues of E2 enzymes in the reduced state, supporting for the formation of protein-ubiquitin conjugates *de novo*(*7*). A rendezvous between E2s and copper signaling pathways has not yet been reported. Here we show that copper signaling is transduced through E2D enzymes, which possess an evolutionarily conserved high-affinity copper-binding CXXXC motif. An allosteric conformational change ensues that increases conjugase activity, markedly accelerating the formation of polyubiquitination and protein turnover, which proves critical for *Drosophila* development.

Cu^+ promotes protein ubiquitination and degradation

While investigating the impact of elevating cellular copper levels in mouse primary cortical neuronal cultures by supplementing media with low concentrations of $CuCl_2$ (Fig. 1A), we were surprised to witness a striking accumulation of polyubiquitinated proteins (Fig 1B). We found similar responses in different cell lines derived from mice (NSC34), rats (N27), hamsters (CHO) and humans (HEK293T) (fig. S1A). Increased polyubiquitination was a dose-dependent response, in tandem with rising intracellular copper levels (fig. S1B). In line with previous reports, such low-dose copper treatment did not impair viability (fig. S2A) or increase reactive oxygen species (fig. S2B)(*8, 9*). Copper imported into the cell is known to rapidly interact with a large excess (millimolar-range) of the major cytosolic redox buffer, GSH, and is then trafficked to designated

cuproproteins(*10*). Such lack of toxicity upon copper supplementation is consistent with the remarkable capacity of cytosolic GSH to hold the free cytoplasmic Cu^+ concentration below 1 fM, even in the face of extreme levels (100 μM) of copper supplementation(*5*). Supporting the conclusion that Cu^+-enhanced polyubiquitination was not a stress-driven phenomenon, exposure of N2a cells to H_2O_2 oxidation could not recapitulate the blush of polyubiquitination induced by copper, and conversely, the antioxidant pyruvate did not attenuate this blush (fig. S2C). Although the proteasome inhibitor MG132 induced a similar blush of polyubiquitinated proteins, across numerous cell lines copper supplementation did not inhibit proteasomal activity (fig. S2D), consistent with previous reports demonstrating proteasome inhibition only at much higher copper concentrations(*11, 12*), which we avoided.

Neither iron and zinc nor cadmium could induce a similar polyubiquitination blush (fig. S3, A and B). Cuprous ions (Cu^+) are rapidly oxidized by dioxygen(*13*), so cupric (Cu^{2+}) salts are routinely used to supplement cell culture media. Some Cu^{2+} can enter the cell via DMT1(*14*) but most Cu^{2+} is reduced at the membrane and transferred into the cytoplasm as Cu^+ by CTR1(*15*). Leveraging this, we stably transfected human CTR1(*16*) into HEK293 cells, finding that this also induced accumulation of polyubiquitinated proteins (Fig. 1C). Thus, a sustained rise in cytoplasmic levels of Cu^+ increases copper-enhanced polyubiquitination. Conversely, treatment with a copper chelator, DiAmSar(*17*), decreased steady-state levels of polyubiquitinated proteins in N2a cells, confirming that under resting conditions, endogenous Cu^+ promotes polyubiquitination under resting conditions (fig. S3C).

To further characterize copper-enhanced polyubiquitination, we added Cu^+ (kept reduced by supplementary GSH) to the post-centrifugation soluble fractions of freshly lysed HeLa cells. The prominent formation of polyubiquitinated proteins within 3 hours in this preparation (Fig. 1D)

could not be explained by a cellular response to protein denaturation or oxidative stress. We then tested the ability of Cu^{+} to modulate the early steps of ubiquitination in a cell-free system containing E1, E2 and E3 enzymes, with biotinylated ubiquitin adduct formation as the readout. We studied Fraction II from HeLa S3 lysate, first used to map this pathway(*18*). Fraction II was incubated in 5 mM EDTA for 30 min and desalted to remove all exchangeable metal ions present. As expected, polyubiquitinated protein conjugates were detected upon re-addition of Mg^{2+} and ATP (Fig. 1E). While in the absence of Mg^{2+}/ATP, Cu^{+} (50 μM) did not induce ubiquitin conjugation, Cu^{+} strikingly augmented polyubiquitinated conjugation induced by Mg^{2+}/ATP, while metal ion sequestration by DTPA abolished polyubiquitin conjugation (Fig. 1E).

Consistent with its impact in generating polyubiquitinated proteins, copper promoted protein degradation. Following a ^{35}S-cysteine/methionine pulse in primary cortical cultures, copper (10 μM) supplementation during a 30-min chase led to increased secretion of labelled low-molecular weight peptides, reflecting accelerated protein degradation (Fig. 1F). Mirroring this result, pulse-chase autoradiography profiles in NSC34 and MEF cell lines showed that copper treatment accelerated the disappearance of labelled cellular proteins (Fig. 1G, and fig. S4, A and B, respectively) and indicated that copper might promote protein degradation in other cell types (fig. S4C). This increase in protein degradation also mitigated the possibility that the polyubiquitination response was mainly due to inhibition of deubiquitination enzymes by Cu^{+}.

Cu^{+} enhances ubiquitination via E2D conjugases

To pursue the mechanism of Cu^{+}-enhanced polyubiquitination, we characterized the ubiquitome(*19*) in NSC34 cells (fig. S5), which manifested robust increases in polyubiquitination induced by copper (fig. S1A). TUBE-affinity capture of protein ubiquitin-modifications from cell

lysates revealed that supplementation with 10 or 25 μM copper increased cellular pools of ubiquitin-associated proteins (fig. S6A), with 882 of these proteins reliably identified (Table S1, and Data S1). Copper supplementation selectively increased the abundance of a subset (48/882) of these proteins, while signaling the suppression of a smaller subset (18/882) (Fig. 2A, fig. S6, B to D, and Data S2). While cysteine and methionine content among the 48 Cu^+-enhanced ubiquitin-associated proteins was slightly higher compared to the larger group of proteins whose abundance was insensitive to copper, mean mass was not different between the two protein groups (fig. S6E).

To probe the mechanism(s) underlying the selective increase in ubiquitin tagging that was fueling protein degradation, we employed a graph-based analysis of the Cu^+-enhanced ubiquitome, using protein-protein interactions (PPIs) from the STRING database (fig. S5A, and Data S3). Of the ubiquitin-associated proteins that were overabundant in Cu^+-supplemented cells, p53 displayed high connectivity and the highest betweenness-centrality (Fig. 2B, and fig. S6F), reflecting interactions with both proteasomal and non-proteasomal proteins (supplementary text). Building on the assumption that highly connected proteins with a central role in a network's architecture are more likely to be essential to the network's overall function(s)(*20, 21*), this analysis indicated that Cu^+-enhanced ubiquitination of p53 could represent a physiological component of an apparent copper-signaling response.

The breadth of Cu^+-enhanced polyubiquitin tagging rendered an upstream target for Cu^+ signalling (e.g. E2 activation) more likely than a downstream target (e.g. activation of many E3s). We would expect E1 activation (e.g. by Cu^+) to generate a much larger list of polyubiquitination targets than we detected (Fig. 2A). While E3s focus the targeting, E2s also contribute to the target specificity of polyubiquitination(*1, 3, 22, 23*). As p53 dominated the functional network of the Cu^+-enhanced ubiquitome (Fig. 2B), we assessed whether the E2D clade, which has a prominent role in the

regulation of p53(*24*), could mediate the effects of copper (fig. S5B). Using the STRING PPI database, 70 of the 882 ubiquitin-associated proteins were predicted to interact with at least one of the four members (E2D1-4) of this clade (Fig. 2C, and Data S4). Cu^{+}-enhanced ubiquitin-associated proteins were indeed highly enriched among E2D targets compared to non-E2D targets (34% vs 3%, Fig. 2C).

Was copper sensitivity observed with targets of other E2 enzymes? We examined targets of the E2A/B (Rad6A/B) clade, as it is also implicated in p53 ubiquitination(*25, 26*). Copper supplementation yielded a marginal enrichment of ubiquitin-associated proteins among the 47 identified E2A/B targets (fig. S6G, and Data S4), yet ~70% of E2A/B targets could also be tagged by E2Ds. Controlling for joint substrates, interaction with an E2D enzyme was the most prominent predictor of copper enhancement for a given ubiquitin-associated protein (Fig. 2D, and Table S2). The odds of Cu^{+}-enhanced ubiquitination for a protein handled by E2D were ~35-fold greater than proteins handled by other E2s, even after controlling for cysteine and methionine content. We therefore hypothesized that Cu^{+}-enhanced (poly)ubiquitination might be explained by augmented E2D interactions.

To evaluate the contribution of E2Ds to copper-promoted ubiquitination in intact cells, we performed a functional experiment using a commercially available knockout (KO) cell line. E2D1-4 are paralogues (Fig. 3A), and ablation of any one paralogue in Hap1 cells does not impair viability. We chose to examine the effect of copper on the E2D2 KO cell line, as E2D2 has been the most extensively characterized, and its expression in myeloid cells is higher than other E2Ds (Table S3). Like all other cell lines tested, copper induced a polyubiquitination blush in the Hap1 cells, but this blush was attenuated in the E2D2 KO cells compared to parental controls (fig. S7A).

Consistent with this, Cu^{+}-induced protein degradation was also diminished in the E2D2 KO cells (fig. S7B).

These results impelled us to evaluate the overall contribution of the E2D clade to copper-promoted ubiquitination in cells. We reduced the expression of all four E2D paralogues by using small interfering RNA (siRNA)-mediated knockdown and examined three different human cell lines (HEK, Fig. 3, B and C; HepG2 and HeLa, fig. S7, C and D, respectively). 48 hours post-transfection, siRNA efficiently suppressed (~75%) E2D1-4 protein expression across cell lines (Fig. 3B, and fig. S7, C and D). Subsequently, copper (2.5-5 μM) was added to the cultures, which were then harvested after 3 hours of incubation. While in control-siRNA-transfected cells copper treatment promoted polyubiquitination, upon E2D1-4 suppression this effect was markedly attenuated (Fig. 3C, and fig. S7, C and D). The viability of the cells at the time of harvesting was not affected by the various interventions (fig. S7E). These findings highlight a key role for the E2D clade in mediating the promotion of polyubiquitination by copper.

Since the E2D subfamily is predominant in directing degradation of p53(*24*) and our ubiquitomics analysis identified p53 as a central target for Cu^{+}-enhanced ubiquitination in NSC34 cells (Fig. 2B, and fig. S6F), we tested whether diminished p53 levels upon copper supplementation could be demonstrated in additional cell lines. In HEK293 cells, copper supplementation (10 μM, 3h) conspicuously enhanced p53 polyubiquitination while promoting its degradation (Fig. 3, D to F, and fig. S7F). This p53 polyubiquitination was unlikely to reflect a stress response (e.g., to oxidation) because a contrasting increase in p53 levels was reported when cells had been intoxicated with 10-20-fold greater copper concentrations(*27-29*) or with a Cu-ionophore(*30*). Nevertheless, we still considered the possibility that the low levels of copper we employed could be oxidizing cysteine residues within p53. To assess this, we used AMS, a reagent that binds non-

oxidized cysteines, inducing a small electrophoretic shift(*31*). We found that AMS binding enhanced p53 immunoreactivity and confirmed that the p53 degradation induced by copper at a non-toxic concentration occurred without cysteine oxidation (Fig. 3E).

Assessing cycloheximide-treated HEK293 cells, prominent copper-induced degradation of p53 was evident in both cytosolic and nuclear fractions (Fig. 3F), confirming the absence of stress-associated nuclear translocation of p53(*27*). Notably, these copper-mediated effects are consistent with enhanced activity of E2D conjugases, which promote polyubiquitination of p53 to designate it for proteasomal degradation, rather than with enhanced activity of UBE2A/B conjugases, which promote p53 monoubiquitination to regulate p53 activity and localization(*32*). A reciprocal accumulation of polyubiquitinated proteins and degradation of p53 was also observed with mouse and human fibroblasts supplemented with copper (fig. S7G), indicating that copper signaling might be a general mechanism to control the levels of p53 in mammalian cells.

E2D conjugases contain an allosteric Cu^+ binding site

E2D1-4 are paralogues, and we thus focused on E2D2 (UbcH5b), as it is the best characterized among the clade and the main conjugation enzyme for p53(*24*). To simulate cytoplasmic conditions in a cell-free assay, we appreciated that although total intracellular copper is ~10 µM, it is largely bound to abundant proteins such as metallothioneins and SOD1 and trafficked through affinity gradients(*10*). Cytoplasmic exchangeable copper is maintained predominantly in its reduced (Cu^+) form, and its maximum free concentration is typically kept in the sub-fM range, by exchange with millimolar concentrations of GSH(*5, 33*). By mimicking the physiological excess of GSH, we established a cell-free functional assay suitable for assessing Cu^+-interactions at ~fM concentrations (fig. S8A). Under these conditions, Cu^+ markedly promoted the activity of

recombinant human E2D2, as measured by the formation of ubiquitin adducts resistant to reducing conditions (Fig. 4A).

We next adopted a site-directed mutagenesis strategy to map the putative Cu^+-binding site responsible for Cu^+-enhanced polyubiquitination. Sequence inspection of the human E2D clade (Fig. 3A), and structural inspection of E2D2 (pdb: 2ESK, Fig. 4, B and C), identified two putative Cu^+-binding regions: i) three cysteines (C21, C107 and C111) ± M38, and ii) two histidines (H32 and H55). Using the functional cell-free assay, both C107 and C111 were critical for Cu^+-enhancement of E2D2 conjugation activity, but C21, M38 and H55 were not (Fig. 4D, and fig. S8B; supplementary text). In solutions where free Cu^+ was kept at picomolar (pM) concentrations by buffering with excess ferrozine (Fz) ligand(*34*), E2D2 bound three Cu^+ ions (Fig. 4, E to H, and fig. S8C). This binding stoichiometry remained unchanged for H55L and C85S mutants (Fig. 4H), indicating that the putative binding site of H32/H55 was too weak to bind Cu^+ under these conditions, and that the active site C85, as expected, was not involved in Cu^+ binding. Both C21S and C111S mutants could bind two Cu^+ ions only, whereas the C107S mutant could bind just one, and a triple mutant (all three Cys → Ser) retained less than 0.4 Cu^+ on average (Fig. 4, E and H). The saturated Cu^+ stoichiometry of the M38L mutant was only slightly less than that of wild-type (WT, Fig. 4H). Consequently, the Cu^+-binding sites with sub-pM affinities are confined to the perimeter defined by C21, C107, C111 and M38 only (Fig. 4C).

Next, Cu^+ affinities of WT E2D2 and the C21S, C21/85S, C107S, C111S and M38L mutants were quantified with the chromophoric probe $Cu^I(Bcs)_2$ under anaerobic conditions. This probe, which buffers free Cu^+ in the sub-fM range(*34*), detected that WT E2D2 competed for binding of two Cu^+ ions cooperatively with an average K_D ~0.5 fM and a Hill coefficient of ~1.6 at pH 7.4 (Fig. 4, F, G and H). Mutation of M38L resulted in only a slight loss of affinity. C21S (or C21/85S)

mutation increased both binding affinity and Hill coefficient, presumably due to the loss of the third weak site associated with C21. In contrast, mutation of either C107S or C111S markedly attenuated Cu^+-binding affinity. Thus, the $C_{107}XXXC_{111}$ region, a consensus motif for Cu^+-coordination(*35*), is the sub-fM Cu^+ binding site of E2D2 (Fig. 4I).

Cu^+ binding at the $C_{107}XXXC_{111}$ motif induces allosteric conformational changes

To assess the conformational changes induced by high-affinity Cu^+-binding, we examined two protein variants, $E2D2_{C21/85S}$ and $E2D2_{C111S,}$ using 2D NMR spectroscopy (Fig. 5, and Table S4). C21S mutation increased the protein solubility in the presence of Cu^+ at the protein concentrations required for the NMR experiments but the mutant retained both high-affinity Cu^+-binding and Cu^+-promoted enzyme activity (Fig. 4, D and F). Compared to C21S, there was no loss of Cu^+-binding affinity or stoichiometry in the $E2D2_{C21/85S}$ form (Fig. 4H), disqualifying Cu^+ interactions with the active site C85. In contrast, C111S mutation ablated both high-affinity Cu^+-binding and Cu^+-promoted enzyme activity (Fig. 4, D and F). The experiments were conducted in a cytosolic-mimicking KPi buffer supplemented with mM GSH, which limits free Cu^+ to sub-fM level through cooperative assembly of a $Cu^I_4(GS)_6$ cluster[5].

The Cu^+-free samples of both E2D2 mutants exhibited well-dispersed ^1H-^{15}N HSQC spectra similar to WT(*36*) (Fig. 5, A and D), confirming minimal impact of the point mutations (C21S, C85S, C111S) on the 3D structure. Addition of Cu^+ into $E2D2_{C21/85S}$, with free Cu^+ buffered by GSH to sub-fM levels, induced conspicuous ^{15}NH chemical shifts of many residues including the well-resolved resonances of N77 and L86 in the active-site region (Fig. 5, A to C). $E2D2_{C21/85S}$ maintained solubility as the Cu^+:protein ratio was increased from 1:1 to 2.5:1. In contrast, addition of Cu^+ into $E2D2_{C111S}$ (1:1) under comparable conditions caused negligible change of the overall

^{1}H-^{15}N HSQC spectrum (Fig. 5, D to F), except for a few resonances that appeared to have derived some minor new features, such as at L86 (~22% protein proportion). Increasing the Cu^{+}:E2D2$_{C111S}$ ratio to 2.5:1 (Fig. 5, E and F), surpassed the buffering capacity of GSH (Table S4) and led to visible protein precipitation with detectable loss of the overall spectral intensity. Nonetheless, the total spectrum of the remaining soluble E2D2$_{C111S}$ remained largely unchanged (Fig. 5, E and F). These experiments demonstrated that: (i) E2D2$_{C21/85S,}$ with an intact $C_{107}XXXC_{111}$ motif, competed with GSH for Cu^{+} effectively, but E2D2$_{C111S}$ competed only weakly under the same conditions, consistent with its attenuated binding affinity (Fig. 4F); (ii) high affinity Cu^{+}-binding to the $C_{107}XXXC_{111}$ motif led to considerable overall tertiary conformational change that might be the basis for the increased enzyme activity; (iii) the weak Cu^{+}-binding to E2D2$_{C111S}$ likely involves C21 as a coordinating residue but led to protein denaturation, which, we hypothesize, might be intended to abort E2D activity in the face of excess copper.

The well-resolved NH resonances of N77 and L86 residues, proximal to the active site C85 but distant from the remote high-affinity Cu^{+}-binding motif $C_{107}XXXC_{111}$ (Fig. 5G), were used for protein speciation analysis. Two allosteric changes induced by the Cu^{+}-binding to this motif were discernible and quantified by the peak height of each species as a fraction of the sum of the peak heights of all protein species (Fig. 5C, Fig. S8D, and Table S4): (i) upon addition of 0.5-equivalent of Cu^{+}, 24% of the N77 and L86 resonance peak heights in the E2D2$_{C21/85S}$ apo-protein (apoP) shifted to another discrete state we defined as "CuP", as well as a second, less abundant (~2%), shifted state we defined as "Cu_2P"; (ii) titrating in more Cu^{+} converted increasing fractions of apoP to CuP and Cu_2P, with the latter increasing in higher proportion, consistent with a process of sequential binding of two Cu^{+} ions to the same $C_{107}XXXC_{111}$ motif (fig. S8D). A detailed protein speciation analysis and estimation of the associated free Cu^{+} concentration under each sample

condition allowed derivation of two Cu^+ dissociation constants, K_{D1} = 0.52 ± 0.02 fM and K_{D2} = 0.45 ± 0.02 fM at pH 7.4, which described this sequential Cu^+-binding process (Fig. 4I, and Table S4). Notably, both K_D values were sub-fM, differed only marginally, and matched the average K_D = 0.21 ± 0.05 fM determined with $Cu(Bcs)_2$ at same pH (Fig. 4H). This rationalizes our interpretation that both CuP and Cu_2P species are in equilibrium with apoP as additional Cu^+ is loaded (fig. S8D), and reprises the 2:1 Cu^+-binding stoichiometry of the high-affinity di-Cys metal-binding motif in the N-terminal domains of HMA2/4 proteins from *Arabidopsis thaliana*(*37*).

Resonances of CuP species that could be assigned while demonstrating resolvable chemical shift changes from apoP were scattered throughout the total spectra (Fig. 5A). These were mapped onto the primary protein sequence (fig. S8E) and the reported 3D structure (Fig. 5G). Notably, these large chemical shift changes triggered by high-affinity Cu^+-binding at $C_{107}XXXC_{111}$ radiated to the proximity of the E2D2 active site (C85), possibly through a pathway across the four antiparallel β-strands (Fig. 5G) which comprise the regulatory backside-binding site(*38*) (supplementary text). The well-resolved peptide NH of N77 and L86, and the sidechain NH_2 of N77, showed clear chemical shift changes on titration with Cu^+ (Fig. 5, A to C). Considering that N77 forms a critical groove that tethers ubiquitin tightly to E2, so that it is primed for nucleophilic attack(*39, 40*), the NMR shift of N77 and nearby residues highlights the allosteric relevance of Cu^+-binding at $C_{107}XXXC_{111}$. Together with the structure-activity relationships (Fig. 4, D to H), our findings indicate that the high-affinity Cu^+-binding coordinated by C107 and C111 mediates the allosteric activation of E2D2 (Fig. 4D). Notably, the sequential Cu^+-binding of apoP → CuP → Cu_2P triggers distinct chemical shift changes for several residues near the Cu^+-binding site including M38, N41 and D42 and also transmits allosterically to distant residues near the C85 active site, including N77, L86 and D87 (Fig. 5, A and B). Therefore, Cu^+-loading of the binding site can induce

augmented levels of remote structural modification at the active site vicinity and, thus, tunable levels of allosteric regulation.

In the presence of Cu^+, the NH resonances of the $XC_{107}XXXC_{111}X$ motif (I106 to D112) could not be reassigned in the triple resonance experiments. No Cα/Cβ connectivities were detected that could be assigned to this region for either the apoP or CuP species, even though the NH resonances of S108, L109, L110 and C111 were well resolved. The lack of Cα/Cβ connectivities implies line-broadening that we attributed to a facile Cu^+-exchange process (with GSH) that shuttled the protein rapidly between the three states (apoP, CuP, Cu_2P) mediated by two similar sub-fM K_D interactions (fig. S8D). However, peak intensities of residues 108-111 were significantly attenuated (30 to 40% of the original intensity; fig. S8F), similar to other resonances affected by Cu^+, and consistent with Cu^+-inducing chemical shifts. As these residues constitute E2D2's α-2 helix, against which the I44 hydrophobic patch of ubiquitin packs, structural modification of this helix upon Cu^+-binding could enhance enzyme activity by stabilizing ubiquitin in the closed conformation(*38*).

Notably, transferring ubiquitin from E2s to their target(s) usually involves a complex with an E3 ligase. To assess whether the proposed sub-fM affinity Cu^+-binding site at $C_{107}XXXC_{111}$ could be accessible in this context, we inspected an available structural model of a relevant E2-E3 dimeric complex $(E2D2\text{-}Ub\text{-}MDM2)_2$ (fig. S9A(i))(*40*). The structure revealed that the $C_{107}XXXC_{111}$ motif was located on the opposite side to the active C85 site (fig. S9A(ii)). The C111 thiol is exposed on the protein surface and is solvent-accessible, yet the C107 thiol appears to be buried by ubiquitin (fig. S9A(iii)). However, a closer inspection of the E2D2-ubiquitin crystal structure (PDB: 3a33)(*41*), stabilized by mutating E2D2-C85S (which enables a stable peptide bridge with ubiquitin's G76, to E2D2's target; fig. S9A(iv), left), revealed that in the absence of MDM2, the ubiquitin unit flipped to the other side of E2D2, partially exposing C107 (fig. S9A(iv), right; the

C107 thiol remains partially buried). Therefore, docking of an E3 ligase should minimally affect solvent accessibility of the $C_{107}XXXC_{111}$ motif, especially given the high flexibility of the ubiquitin orientation relative to E2D2. Considering both structural models, we focused our remaining experiments on C111.

C111 of E2D is a conserved physiological Cu^+ sensor critical for *Drosophila* head formation

We initially tested if endogenous cellular Cu^+ could be mobilized to promote E2D2 activity or whether enhanced activity occurred only during Cu^+ excess. We prepared Hap1 E2D2-KO cell lysates (fig. S9B) and added back recombinant WT E2D2 or C111S mutant enzymes. As expected, recombinant WT E2D2 added to these lysates induced a prominent polyubiquitination blush. This was dose-dependently attenuated by selective, strong Cu^+ chelation (bathocuproine:tetrathiomolybdate, 1:1), demonstrating that endogenous Cu^+ indeed amplified the polyubiquitination. In contrast, application of recombinant Cu^+-insensitive C111S mutant only modestly enhanced polyubiquitination in the lysate, and attenuation of the blush upon Cu^+ chelation was muted, indicating that E2D2's Cu^+-sensitivity is physiologically relevant.

Among the human E2 family, the Cu^+-binding residues C107 and C111 constitute a unique signature of the E2D clade (fig. S10A). Despite relative conservation of E2D orthologs(*42*), the $C_{107}XXXC_{111}$ Cu^+-binding motif is not evident in non-holozoan lineages (fig. S10B, and Data S5). Absent also in unicellular holozoans, yet present across main metazoan lineages, the sub-fM affinity Cu^+-binding site in E2s was likely to emerge in the late Precambrian (Fig. 6A and Data S6; supplementary text). Novel signaling pathways that appeared at the metazoan root often modulate cell fate and morphogenesis by co-opting pre-existing cell proliferation mechanisms(*43*), and given its conservation throughout bilaterian evolution (Fig. 6A), we explored its

developmental relevance in the fruit fly. Short of the four-paralogue repertoire that evolved in vertebrates, the *D. melanogaster* orthologue UbcD1 (aka Effete) shows a remarkable homology with human E2Ds, especially with E2D2 (fig. S10C, and Data S7).

Using the GAL4/UAS bipartite *in vivo* gene manipulation system with three independent UAS-RNAi lines, we demonstrated that *UbcD1* knockdown: 1) when ubiquitous, caused early larval death, indicating that *UbcD1* is an essential gene; 2) during early head / eye development resulted in complete loss of the head structures; 3) in the central dorsal stripe resulted in a thoracic cleft plus increased pigmentation in affected cells; 4) in the entire central nervous system caused early pupal death; 5) in the CCAP neuropeptide-producing cells caused a failure of normal adult wing expansion; and 6) in the developing eye caused loss and disorganization of the normal ommatidial array (Fig. 6B). These phenotypes could be explained by UbcD1's known roles in promoting apoptosis(*44, 45*), neuronal dendrite pruning(*46, 47*), and Hedgehog pathway signalling(*48*). Remarkably, similar phenotypes have also been associated with copper dysregulation(*49-52*). Moreover, one of UbcD1's known E3 ubiquitin ligase partners, Slmb, has been identified as a novel regulator of copper homeostasis(*48, 53*).

To ascertain the importance of E2D2's Cu^{+}-sensing C111 residue *in vivo*, we generated transgenic *Drosophila* strains allowing the targeted expression of either WT or C111S human E2D2. With all the GAL4 driver lines tested earlier, *h*E2D2^{WT}-expression provided an almost complete rescue of the detrimental phenotypes induced by *UbcD1* knockdown (Fig. 6B), reconfirming the expected functional conservation across species (fig. S10B). However, despite being transcribed at the same levels as *h*E2D2^{WT} (since transgene insertion occurred at the same genomic location), expression of *h*E2D2^{C111S} offered only minimal rescue (Fig. 6B). The hypomorphs were characterized by caspase-3 activation in neuronal tissue (Fig. 6C), indicating that cell death was mediated by

apoptosis. These functional data, which directly link the allosteric Cu^+-sensing $C_{107}XXXC_{111}$ motif of E2D2 with *Drosophila* development and head formation, are concordant with functional pathways that were over-represented in the Cu^+-enhanced ubiquitome (fig. S5C), including regulation of apoptosis (fig. S11, A to D) and cell cycle (Data S8; supplementary text).

Discussion

Copper has only recently been recognised as a potential signalling ion in brain and other tissues(*6*). Direct partial *inhibition* of PDE3B activity by copper binding to C768, located away from the enzyme active site, emerged as the first example of a modulatory Cu^+ binding site(*54*). This was reflected in 3T3-L1 cells, where extracellular copper supplementation (50 μM) potentiated lipolysis. Here we show what, to the best of our knowledge, is the first example of copper signaling inducing an allosteric conformational change that *enhances* enzyme activity. We have delineated an unprecedented confluence between ubiquitin conjugation and copper, interwoven by a unique sub-fM affinity Cu^+-binding site ($C_{107}XXXC_{111}$) on the E2D clade. This tunable switch markedly promotes target polyubiquitination and can thus regulate the degradation rate of many proteins, contributing to development and, notably, head formation in *Drosophila*. While we demonstrated that E2D2 activation is a major component of the copper-induced polyubiquitination blush, and that activation of the E2D clade is likely to mediate much of the protein turnover induced by copper supplementation in cell culture, we have not excluded lesser contributions from other components of the ubiquitin-proteasomal system, including potential interplay between copper and E3 ligases(*55*) or deubiquitinating enzymes(*56*).

The high-affinity Cu^+ allosteric binding site on E2D evolved (Fig. 6A) contemporaneously with increasing copper bioavailability in Neoproterozoic oceans. Ancient geochemical shifts fashioned

metal–protein partnerships(*57*) and, indeed, the appearance of this site might reflect a concurrent transition to copper-based nitrogen assimilation(*58*). In this setting it may have been advantageous for the nascent metazoan kingdom to evolve a Cu^+-signaling mechanism that couples protein turnover with surrounding nitrogen availability. Coinciding with cuproenzyme evolution(*59*), incorporation of the $C_{107}XXXC_{111}$ motif into E2s would link Cu^+ levels with the turnover of p53, which had served a protective role in unicellular holozoans(*60*). With the advent of animal multicellularity, this signaling pathway could tune p53 to control cell fate and organism size(*43*), eventually evolving to influence tissue morphogenesis (Fig. 6B).

The discovery of this novel p53-regulating signaling pathway has broad biomedical implications. Consistent with data showing that copper chelators increase p53(*61*), we found that Cu^+ promoted p53 degradation by allosterically activating E2D2. p53 depletion is a critical initiator of malignancy, and cancer tissue exhibits a mysterious high demand for copper(*4, 6, 62*), with some malignancies (e.g. KRAS-mutated colorectal cancers) harnessing their surfaceome in service of their copper addiction(*63*). Our findings could link increased cancer cell copper uptake with p53 depletion, accounting for the inverse association of tumor copper levels with chemosensitivity and prognosis(*64*). The emerging benefits of copper modulation in cancer treatment(*64, 65*) could also be explained via this novel p53-regulating signaling pathway. Unlike cancer, major neurodegenerative disorders are complicated by low tissue copper concentrations(*66-68*) and ubiquitinopathy alongside elevated p53(*69*). Based on our findings, decreasing total brain copper levels with advancing age(*70*) or neurodegeneration could elevate p53 and impair proteostasis. The cause of age- and disease- dependent brain copper supply failure is uncertain, but is unlikely to be corrected nutritionally(*71*), as Cu^+ does not passively cross the blood-brain-barrier. The

present data indicate that correction of defective proteostasis could underly the enigmatic potential of copper chaperones to rescue neurodegeneration(*72*).

Fig. 1

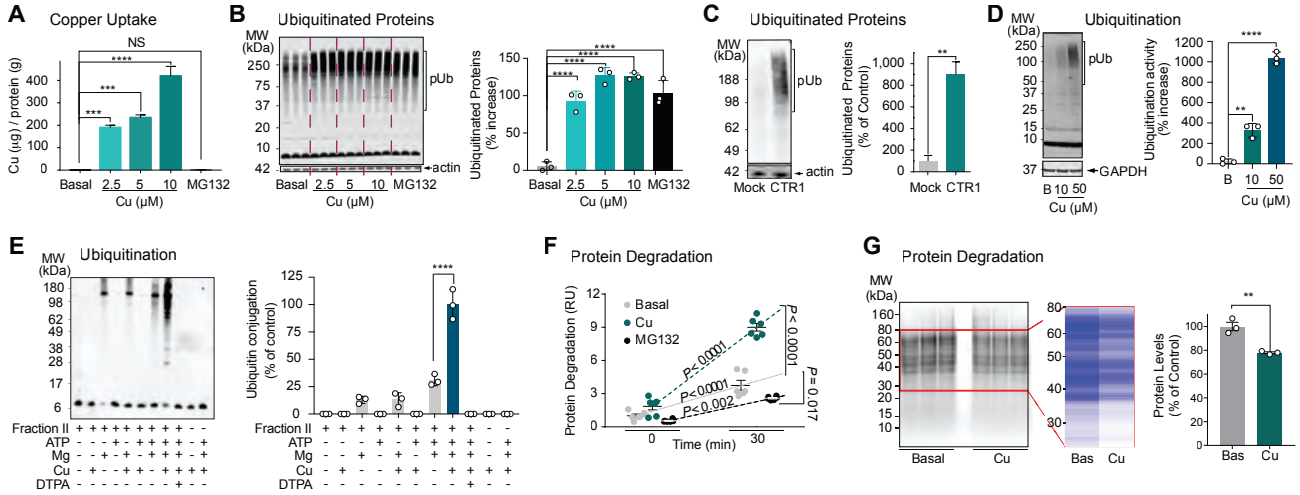

Fig. 1. Cu^{+} promotes protein ubiquitination and degradation.

(**A)** Cellular copper levels following supplementation. Primary cortical neurons were untreated (basal) or supplemented with $CuCl_2$ (Cu; up to 10 μM) for 3 h in Locke's media. (**B**) Ubiquitination response to copper supplementation in primary cortical neuronal cells. Ubiquitinated proteins (pUb) were detected by blot (P4D1 antibody). Actin was used as loading control. Data in **A** and **B** are means ± SEM (n = 3). **P*<0.05, ***P*<0.01, ****P*<0.001, *****P*<0.0001, ANOVA followed by Dunnett's test. (**C**) Levels of pUb in HEK-CTR1 (stably transfected) and HEK-mock cells. *P* value is from independent samples *t*-test. (**D**) Copper promotes ubiquitination in freshly lysed HeLa cell supernatants. Cell supernatants were incubated in the absence (basal=B) or presence of $CuCl_2$ (10 and 50 μM, in 200 μM GSH + 50 mM Tris-HCl, pH 7.5) for 3h. Ubiquitinated proteins were detected by blot (P4D1 antibody). GAPDH was used as loading control. Data are means ± SEM (n = 3). ***P*<0.01, *****P*<0.0001, ANOVA followed by Tukey's test. (**E**) Copper activates polyubiquitination *in vitro* using Fraction II as a source of E-enzymes. Fraction II (the protein fraction of HeLa S3 lysate that binds to anion exchange resin) was firstly incubated in 5 mM EDTA for 30 min and desalted, then incubated with biotinylated ubiquitin (2.5 μM) in the presence or absence of ATP (2 mM), $MgCl_2$ (5 mM), $CuCl_2$ (50 μM) and DTPA (5 mM) at 37 ºC for 5 h. Other components include: DTT (1 mM), creatine phosphate (10 mM), creatine phosphokinase (0.6 U), and inorganic pyrophosphatase (0.6 U). Samples were submitted to electrophoresis under non-reducing conditions. The formation of ubiquitin conjugates was detected by binding of avidin-HRP using ECL detection system. The graph summarizes data obtained in three different experiments. Data are means ± SEM. **** *P* <0.0001. (**F**) Copper promotes protein degradation. Primary cortical neuronal cells were labelled with ^{35}S-Cys/Met for 1 h, followed by chase in unlabeled media containing cycloheximide ± $CuCl_2$ (10 μM) or MG132 (50 μM) for 30 min. The

graph shows an index of protein degradation (radioactive counts from the media that remain soluble after TCA precipitation = peptide fragments / counts from total cell proteins). Data are means ± SEM (n = 6). Two-way-ANOVA followed by Tukey's and Sidak's tests. (**G**) NSC34 cells were labelled with ^{35}S-Cys/Met, followed by chase in unlabeled media containing cycloheximide ± $CuCl_2$ (10 µM) for 30 min. Autoradiography protein profile upon gel electrophoresis of triplicate cell cultures is shown. The red frame encloses a region of interest, represented as an intensity heatmap for 120 equal bins averaged across each experimental condition. Graphed data show means ± SEM (n = 3) with independent-samples *t*-test.

Fig. 2

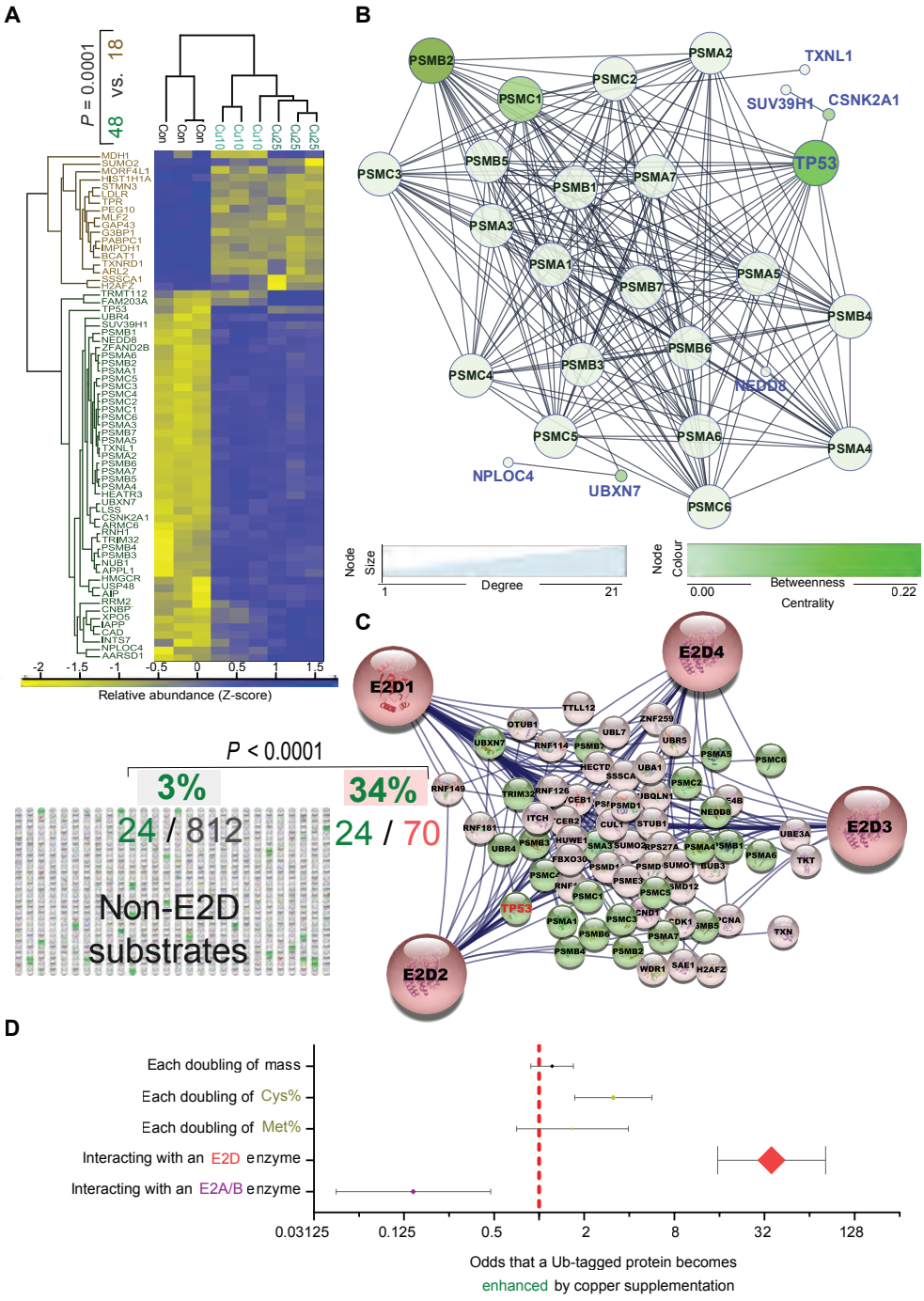

Fig. 2. Cu^{+} enhances E2D-mediated ubiquitination.

NSC34 cells were treated ± $CuCl_2$ (10 μM, 25 μM) for 3 h, and harvested for ubiquitomics. (**A**) Heatmap depicting the relative abundance (standardized per protein) of 66 ubiquitin-associated proteins whose abundance was altered by copper ($q<0.01$, ANOVA followed by permutation-based-FDR). 48 ubiquitin-associated proteins were over-abundant in Cu^{+}-supplemented media, compared with 18 that were over-abundant in control media. Dendograms depict hierarchical clustering according to media conditions (columns; three replicates per condition) and protein abundance profile (rows). (**B**) Cu^{+}-enhanced ubiquitome. A connected subnetwork of 27 proteins (nodes) that displayed over-abundance in Cu^{+}-supplemented media was generated using STRING protein-protein interactions database. Size and colour correspond to node-degree and betweenness-centrality, respectively. (**C**) Enrichment analysis comparing the proportion of proteins displaying Cu^{+}-enhanced over-abundance (green nodes) among STRING-predicted E2D substrates (right side) versus the corresponding proportion among non-E2D substrates (left side), using Fisher's exact test. (**D**) Effects of protein mass, redox-sensitive amino acids, and being a E2D or E2A/B substrate, on Cu^{+}-enhanced ubiquitination. Using multiple logistic regression, odds (*x*-axis, log_2-scale) ± 95% CI of a ubiquitin-associated protein becoming over-abundant upon copper supplementation were estimated for each doubling of protein mass or cysteine/methionine content, or for being a E2D or E2A/B substrate. Diamond sizes reflect Wald-statistic of each predictor.

Fig. 3

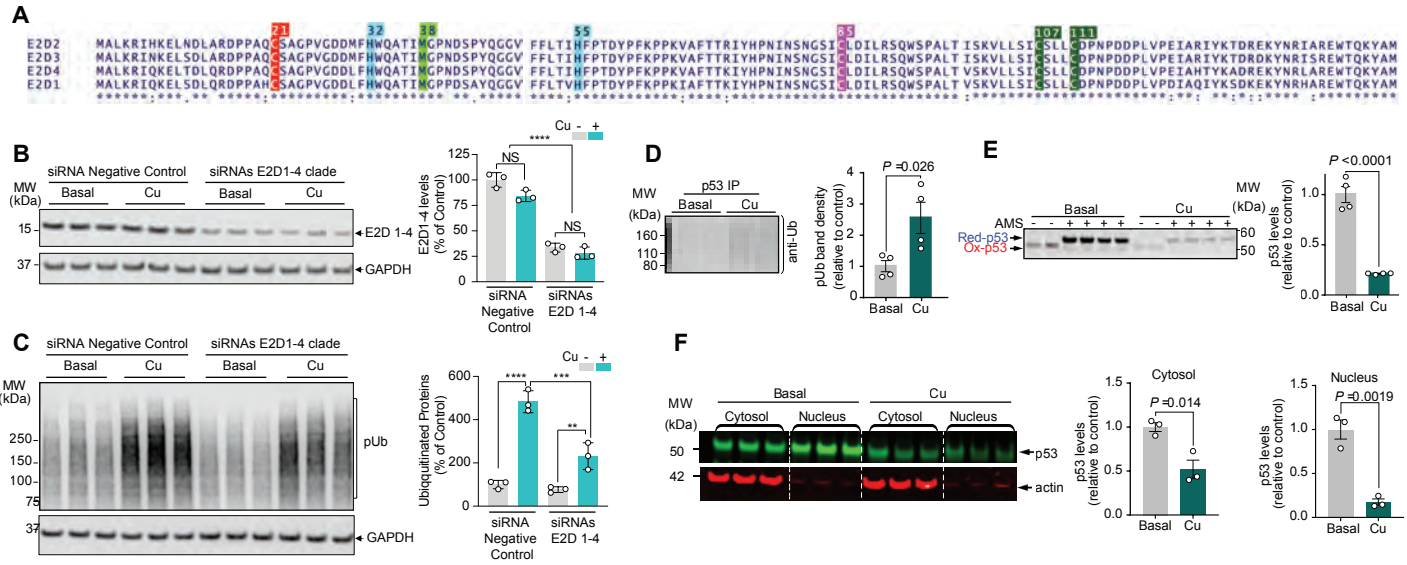

Fig. 3. E2D clade is key for Cu^{+}-promoted ubiquitination.

(**A)** Sequence alignment of E2D1-4 proteins. The C85 is the enzyme active site. Other highlighted residues are the potential Cu^{+} ligands. Residues shared by all four paralogues are denoted with an asterisk. (**B-C**) HEK293 cells were treated with control siRNA or siRNA against E2D1-4 for 48h. Then cells were untreated (basal) or supplemented with $CuCl_2$ (Cu; 2.5 μM) for 3 h in Locke's media. (**B**) The levels of E2D1-4 were detected with an antibody that recognizes the full E2D clade. (**C**) Ubiquitinated proteins (pUb) were detected by blot (P4D1 antibody). GAPDH was used as loading control. Data in **B** and **C** are means ± SEM (n = 3). ***P*<0.01, ****P*<0.001, *****P*<0.0001, ANOVA followed by Bonferroni's test. (**D**) Copper promotes ubiquitination and degradation of p53. HEK293 cells were incubated ± $CuCl_2$ (10 μM) for 3h, and ubiquitinated p53 was immunoprecipitated by anti-p53 antibody and blotted with anti-Ub antibody (DAKO). The blot from duplicate cultures illustrates the boost in polyubiquitinated p53 induced by copper (full blot presented in fig. S7F). (**E**) Western blot for p53 in the same experiment shows that copper promoted the degradation of p53. Densitometry data are means ± SEM (n=4). AMS (4′-acetamido-4′-maleimidylstilbene-2,2′-disulfonic acid), which binds reduced cysteine residues in the extract, generated an electrophoretic shift, confirming no oxidation of these residues in p53. (**F**) p53 Western blot of nuclear and cytosolic fractions of these cells reveals that copper induces both cytosolic and nuclear p53 loss. Actin was used as loading control. Densitometry data are means ± SEM (n=3), with independent-samples *t*-tests.

Fig. 4

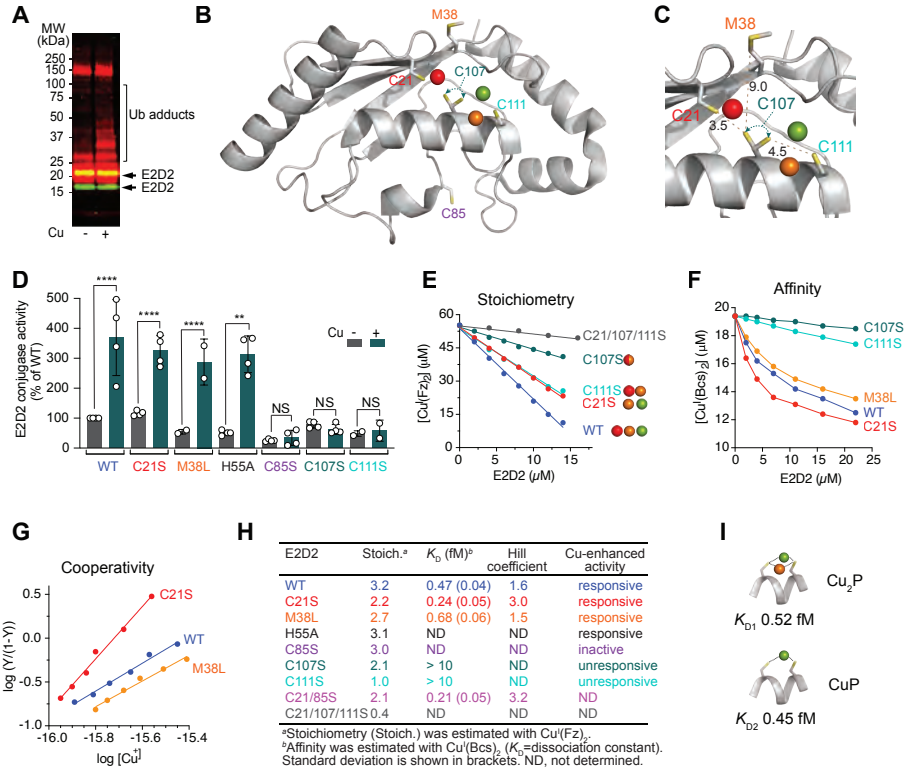

H

E2D2	Stoich.[a]	K_D (fM)[b]	Hill coefficient	Cu-enhanced activity
WT	3.2	0.47 (0.04)	1.6	responsive
C21S	2.2	0.24 (0.05)	3.0	responsive
M38L	2.7	0.68 (0.06)	1.5	responsive
H55A	3.1	ND	ND	responsive
C85S	3.0	ND	ND	inactive
C107S	2.1	> 10	ND	unresponsive
C111S	1.0	> 10	ND	unresponsive
C21/85S	2.1	0.21 (0.05)	3.2	ND
C21/107/111S	0.4	ND	ND	ND

[a]Stoichiometry (Stoich.) was estimated with $Cu^{I}(Fz)_2$.
[b]Affinity was estimated with $Cu^{I}(Bcs)_2$ (K_D=dissociation constant).
Standard deviation is shown in brackets. ND, not determined.

Fig. 4. Cu^+ is an allosteric activator of E2D2: high affinity Cu^+ binding to E2D2 dictates Cu^+-promoted activity.

Identification of Cu^+-binding ligands and sites in E2D2. (**A**) Biotin blot of cell-free conjugation activity of WT E2D2. The enzyme was incubated ± $CuCl_2$ (5 μM) in the presence of GSH (200 μM), UBA1 (100 nM), $MgCl_2$ (5 mM), ATP (5 mM) and biotinylated-Ub (2.5 μM) in Tris-HCl (50 mM, pH 7.5) at 37 ºC. The reaction was stopped after 1 h by adding TCEP (50 mM). Ubiquitin adducts were detected by Streptavidin-680IR (red signal) and E2D2 (green-yellow signal) was detected by Western blot. Increased ubiquitin tagging (ubiquitin adducts between 25 kDa and 100 kDa) indicated more conjugase activity. (**B**) Crystal structure of E2D2 (pdb: 2ESK). Coloured spheres represent putative sub-pM affinity Cu^+-binding sites. Sidechains of conserved Cys/Met residues are shown as sticks. The sidechain of C107 is shown with two rotamers to reflect the flexibility of the distance between the key Cu^+ ligands. (**C**) Zoom-in view of the high-affinity cooperative Cu^+-binding region, highlighting distances (Å; yellow dashed lines) between the proposed ligands. (**D**) The graph shows the ubiquitin conjugase activity of WT E2D2, or C21S, M38L, H55A, C85S, C107S and C111S mutants (5 μM) in the absence (grey bars) or the presence of $CuCl_2$ (5 μM; green bars) under the same conditions described above. (**E-H**) Quantification of high-affinity Cu^+-binding to E2D2. (**E**) Determination of Cu^+-binding stoichiometry utilizing a pM-affinity probe $Cu^I(Fz)_2$ under non-competitive conditions. Sphere colors correspond to sub-pM affinity Cu^+-binding sites proposed in Fig. 4, A and B. (**F**) Determination of Cu^+-binding affinity of WT E2D2 and selected mutants with sub-fM affinity probe $Cu^I(Bcs)_2$ under competitive conditions. The C107S and C111S mutants compete only weakly for Cu^+-binding under these conditions. (**G**) Hill plots for the sub-fM Cu^+-binding detected by the $Cu^I(Bcs)_2$ probe. (**H**) Table summarizing Cu^+-binding properties and Cu^+-enhanced activities of WT and mutant E2D2

proteins. (**I**) Two different Cu^+-binding states (CuP and Cu_2P) proposed from our NMR study, together with the two derived Cu^+ K_D values (see Table S4).

Fig. 5

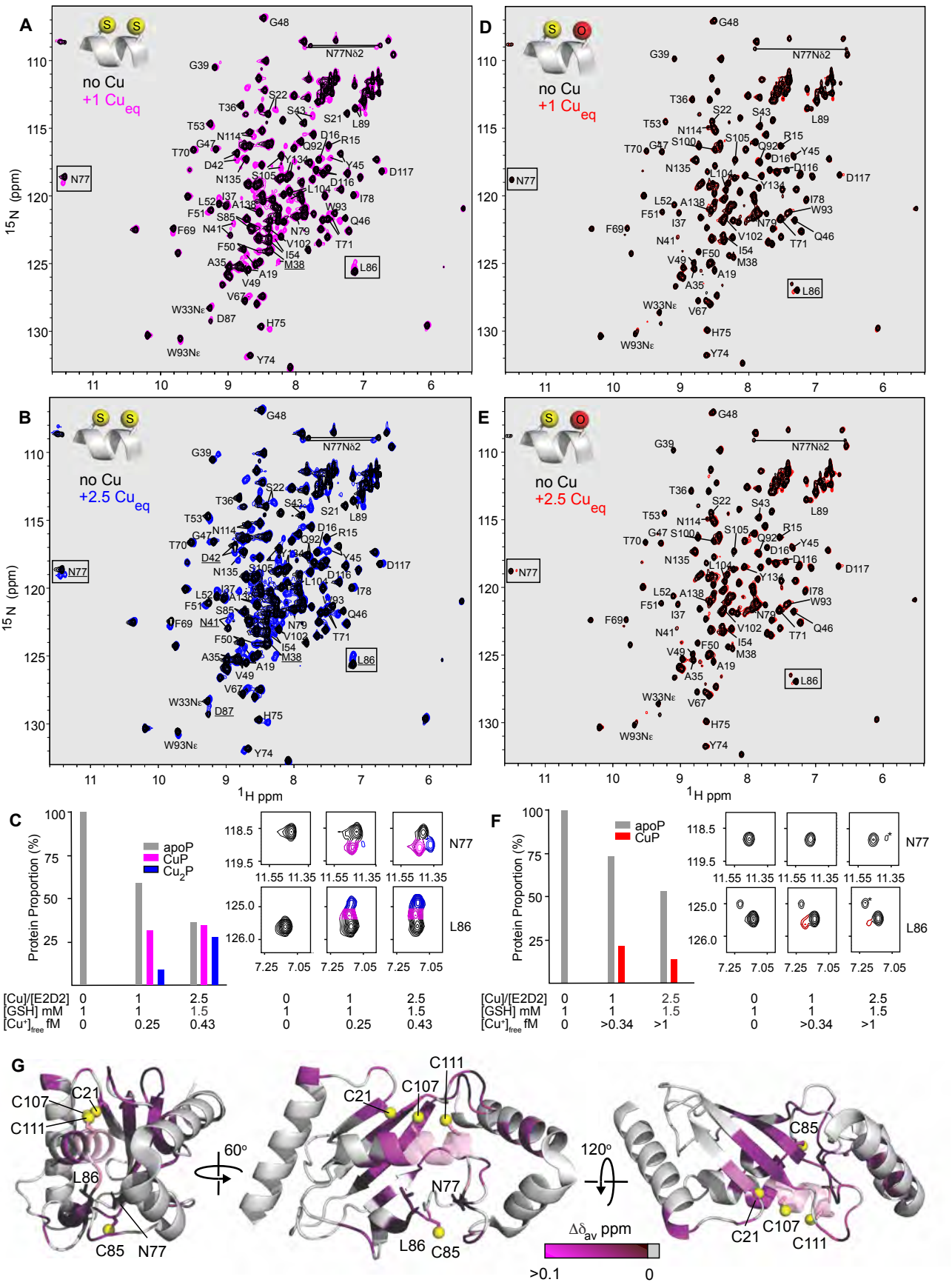

Fig. 5. Allosteric effect of the high-affinity Cu^+-binding to E2D2 detected by NMR spectroscopy.

(**A-B**) Overlay of 2D ^1H-^{15}N HSQC spectra of 0.2 mM $E2D2_{C21/85S}$ without Cu^+ (black) and with 0.2 mM Cu^+ (magenta, **A**) or 0.5 mM Cu^+ (blue, **B**) in 100 mM KPi buffer (pH 7.4), 2.0 mM NH_2OH, 1.0 mM (**A**) or 1.5 mM (**B**) GSH and 5% D_2O. Resonances that show Cu^+-induced chemical shifts and could be assigned to CuP species in the presence of 0.2 mM Cu^+ are indicated in both spectra. These new resonances increased in intensity and/or gave rise to a resolved third peak on the addition of 0.5 mM Cu^+. Several residues showing these three distinct peaks assigned to apoP, CuP and Cu_2P species are underlined and include M38, N41 and D42 near the Cu^+-binding site and N77, L86 and D87 near the active site. The resonances for I106 to D112 are excluded as reassignment was not possible, but they showed significant losses in intensity in the presence of Cu^+ (fig. S8F). Notably, the sidechain NH_2 of N77 and the indole NH of W33 and W93 also show Cu^+-induced chemical shift changes. (**C**) Changes to chemical shift and peak intensity for two well-resolved resonances, assigned to N77 and L86 (spectral expansions in right-hand panels) located near the active site and distant from the Cu^+-binding site. The left-hand panels show the average peak-height changes for the three resonances assigned to the apoP, CuP and Cu_2P species (see Table S4 for detail). (**D-E**) Overlay of ^1H-^{15}N HSQC spectra of 0.2 mM $E2D2_{C111S}$ without Cu^+ (black) and with 0.2 mM Cu^+ (red, **D**) or 0.5 mM Cu^+ (red, **E**) in 100 mM KPi buffer (pH 7.4), 2 mM NH_2OH, 1 mM GSH and 5% D_2O. The resonances for C21, D42, C85, I88, S111, D112, I119, A124 and Y127 of $E2D2_{C111S}$ are excluded as they could not be unambiguously identified. For $E2D2_{C111S}$ there was little Cu^+-induced variation in chemical shift, however, the protein was less stable especially at 2.5:1 [Cu]/[E2D2], precipitating over the course of the experiment resulting in loss of resonance intensity. (**F**) Histogram of peak intensity changes for L86 and

spectral expansions for N77 and L86, equivalent to panel **C**. A weak Cu^{+}-induced peak was observed for L86 at 1:1 [Cu]/[E2D2] that weakened at 2.5:1 but retained similar proportion relative to that of apoP. The loss of intensity is consistent with ~10% and ~40% precipitation for 1:1 and 2.5:1 ([Cu]/[E2D2]), respectively (Table S4). The peaks marked (*) are contaminants that were observed in the absence of Cu^{+}. (**G**) Cu^{+}-induced chemical shift changes in panel A mapped onto the structure of E2D2 (pdb: 2ESK), that show Cu^{+}-allosteric modulation throughout the protein and to the active site. The largest chemical shift differences ($\Delta\delta_{av} > 0.1$ ppm) are in magenta and smaller shifts are shown progressively darkened. The region I106 to D112 is shown in transparent pink. The resonances of this region show significant intensity changes to the apo-state resonance, but reassignment of Cu^{+}-induced shifts was not possible. Values for chemical shift changes are given in fig. S8E. The sulfur atoms of the Cu^{+}-binding ligands C21, C107 and C111 and the active site C85 are shown as yellow spheres. The sidechains of N77 and L86 are also indicated.

Fig. 6

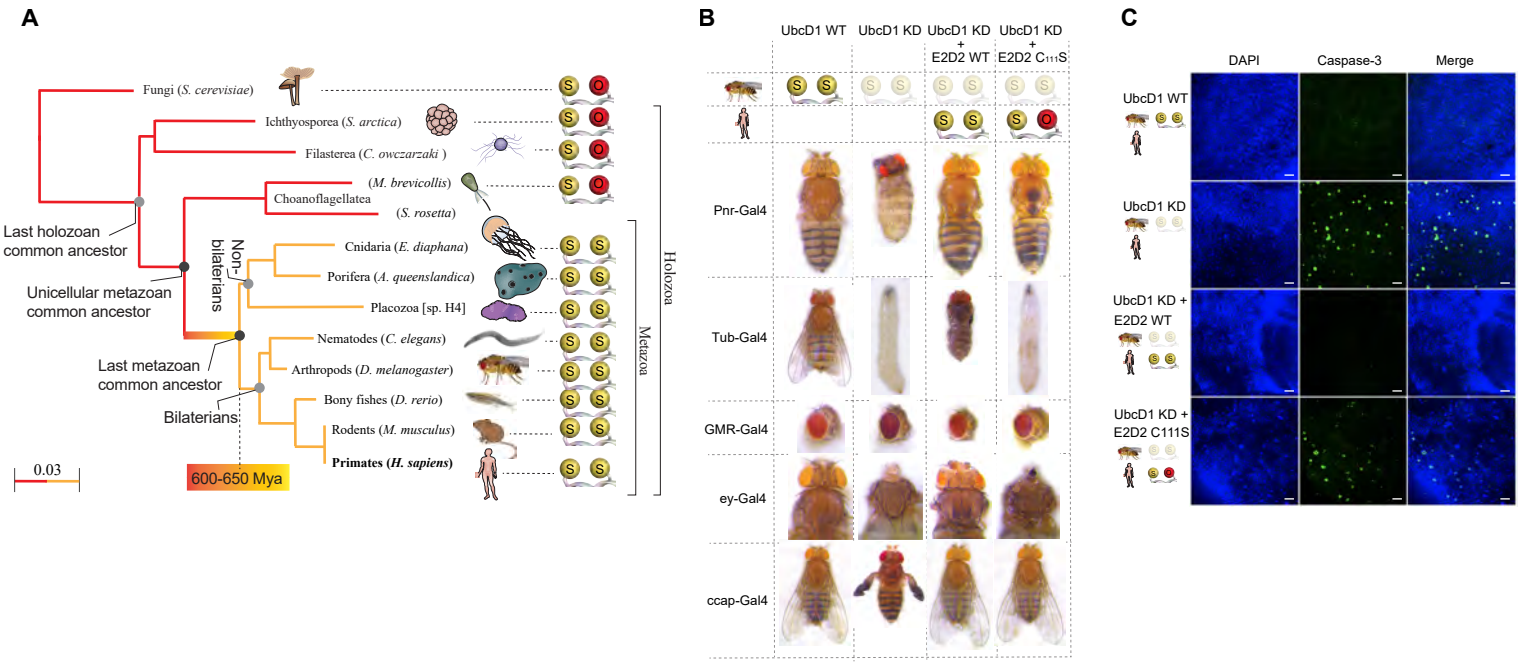

Fig. 6. Evolutionary conserved C111 of E2D2 is key for *Drosophila* head formation.

(**A**) Evolutionary tree of E2D2 orthologues among holozoa. Representative species from major animal lineages and from three independent, closely related, unicellular holozoan lineages were used for generating a Fast Minimum Evolution tree based on Grishin protein distance (scale, left-lower corner), with human E2D2 as reference. Side chain atoms of the Cu^{+}-binding ligands at position 107 (left) and 111 (right) are shown as spheres, coloured yellow (sulfur at C107) and red/yellow (oxygen/sulfur at T/C111, respectively). Appearing only after separation of unicellular and multicellular metazoan lineages, yet evident across multiple animal lineages, emergence of a fully developed Cu^{+} ligand configuration could be timed. (**B**) Phenotypes caused by targeted *UbcD1* knockdown. Control (Gal4 transgene only) are shown on the left. The second column shows the effect of *UbcD1* knockdown in the adult thorax (Pnr-Gal4; cleft and hyperpigmentation), the entire animal (Tub-Gal4; larval lethality), the eye (GMR-Gal4, rough eye), the developing head / eye (Ey-Gal4; complete loss of head structures) and crustacean cardioactive peptide (CCAP)-expressing neurons (CCAP-Gal4; failure of wing expansion). Third column shows rescue by co-expression of human E2D2-WT. Fourth column shows reduced / absent rescue by co-expression of E2D2-C111S. (**C**) Brain sections showing induction of active Caspase 3 in *Ey-Gal4* expressing cells upon knockdown of *UbcD1* in the absence or presence of the expression of E2D2 WT or E2D2 C111S. Sections were stained with DAPI (Blue, nuclear staining) and Caspase-3 activity was determined (green signal). Scale bars represent 10 µm.

References and notes

1. S. J. van Wijk, H. T. Timmers, The family of ubiquitin-conjugating enzymes (E2s): deciding between life and death of proteins. *FASEB journal : official publication of the Federation of American Societies for Experimental Biology* **24**, 981-993 (2010).
2. M. D. Stewart, T. Ritterhoff, R. E. Klevit, P. S. Brzovic, E2 enzymes: more than just middle men. *Cell Res* **26**, 423-440 (2016).
3. J. D. Wright, P. D. Mace, C. L. Day, Noncovalent Ubiquitin Interactions Regulate the Catalytic Activity of Ubiquitin Writers. *Trends in Biochemical Sciences* **41**, 924-937 (2016).
4. M. L. Turski, D. J. Thiele, New Roles for Copper Metabolism in Cell Proliferation, Signaling, and Disease. *Journal of Biological Chemistry* **284**, 717-721 (2009).
5. M. T. Morgan, L. A. H. Nguyen, H. L. Hancock, C. J. Fahrni, Glutathione limits aquacopper(I) to sub-femtomolar concentrations through cooperative assembly of a tetranuclear cluster. *J Biol Chem* **292**, 21558-21567 (2017).
6. C. M. Ackerman, C. J. Chang, Copper Signaling in the Brain and Beyond. *Journal of Biological Chemistry*, (2017).
7. J. Jahngen-Hodge, M. S. Obin, X. Gong, F. Shang, T. R. Nowell, Jr., J. Gong, H. Abasi, J. Blumberg, A. Taylor, Regulation of ubiquitin-conjugating enzymes by glutathione following oxidative stress. *J Biol Chem* **272**, 28218-28226 (1997).
8. S. Sánchez Campos, G. Rodríguez Diez, G. M. Oresti, G. A. Salvador, Dopaminergic Neurons Respond to Iron-Induced Oxidative Stress by Modulating Lipid Acylation and Deacylation Cycles. *PLoS ONE* **10**, e0130726 (2015).
9. K. Shimada, E. Reznik, M. E. Stokes, L. Krishnamoorthy, P. H. Bos, Y. Song, C. E. Quartararo, N. C. Pagano, D. R. Carpizo, A. C. deCarvalho, D. C. Lo, B. R. Stockwell, Copper-Binding Small Molecule Induces Oxidative Stress and Cell-Cycle Arrest in Glioblastoma-Patient-Derived Cells. *Cell Chemical Biology* **25**, 585-594.e587 (2018).
10. L. Banci, I. Bertini, S. Ciofi-Baffoni, T. Kozyreva, K. Zovo, P. Palumaa, Affinity gradients drive copper to cellular destinations. *Nature* **465**, 645-648 (2010).
11. M. Amici, K. Forti, C. Nobili, G. Lupidi, M. Angeletti, E. Fioretti, A. Eleuteri, Effect of neurotoxic metal ions on the proteolytic activities of the 20S proteasome from bovine brain. *JBIC Journal of Biological Inorganic Chemistry* **7**, 750-756 (2002).
12. A. M. Santoro, I. Monaco, F. Attanasio, V. Lanza, G. Pappalardo, M. F. Tomasello, A. Cunsolo, E. Rizzarelli, A. De Luigi, M. Salmona, D. Milardi, Copper(II) ions affect the gating dynamics of the 20S proteasome: a molecular and in cell study. *Scientific Reports* **6**, 33444 (2016).
13. R. D. Gray, The Kinetics of Oxidation of Copper (I) by Molecular Oxygen in Perchloric Acid-Acetonitrile Solutions. *Journal of the American Chemical Society* **91**, 56-62 (1969).
14. W. Zheng, A. D. Monnot, Regulation of brain iron and copper homeostasis by brain barrier systems: Implication in neurodegenerative diseases. *Pharmacology & Therapeutics* **133**, 177-188 (2012).
15. A. Dancis, D. S. Yuan, D. Haile, C. Askwith, D. Eide, C. Moehle, J. Kaplan, R. D. Klausner, Molecular characterization of a copper transport protein in S. cerevisiae: an unexpected role for copper in iron transport. *Cell* **76**, 393-402 (1994).

16. B. Zhou, J. Gitschier, hCTR1: a human gene for copper uptake identified by complementation in yeast. *Proceedings of the National Academy of Sciences* **94**, 7481-7486 (1997).
17. H. McArdle, S. Gross, I. Creaser, A. Sargeson, D. Danks, Effect of chelators on copper metabolism and copper pools in mouse hepatocytes. *American Journal of Physiology-Gastrointestinal and Liver Physiology* **256**, G667-G672 (1989).
18. A. Ciehanover, Y. Hod, A. Hershko, A heat-stable polypeptide component of an ATP-dependent proteolytic system from reticulocytes. *Biochemical and biophysical research communications* **81**, 1100-1105 (1978).
19. S. R. Nagarajan, A. E. Brandon, J. A. McKenna, H. C. Shtein, T. Q. Nguyen, E. Suryana, P. Poronnik, G. J. Cooney, D. N. Saunders, A. J. Hoy, Insulin and diet-induced changes in the ubiquitin-modified proteome of rat liver. *PloS one* **12**, e0174431 (2017).
20. H. Jeong, S. P. Mason, A. L. Barabasi, Z. N. Oltvai, Lethality and centrality in protein networks. *Nature* **411**, 41-42 (2001).
21. A.-L. Barabasi, Z. N. Oltvai, Network biology: understanding the cell's functional organization. *Nat Rev Genet* **5**, 101-113 (2004).
22. Dawn M. Wenzel, Kate E. Stoll, Rachel E. Klevit, E2s: structurally economical and functionally replete. *Biochemical Journal* **433**, 31-42 (2011).
23. Y. Ye, M. Rape, Building ubiquitin chains: E2 enzymes at work. *Nat Rev Mol Cell Biol* **10**, 755-764 (2009).
24. M. K. Saville, A. Sparks, D. P. Xirodimas, J. Wardrop, L. F. Stevenson, J.-C. Bourdon, Y. L. Woods, D. P. Lane, Regulation of p53 by the Ubiquitin-conjugating Enzymes UbcH5B/C in Vivo. *Journal of Biological Chemistry* **279**, 42169-42181 (2004).
25. A. Lyakhovich, M. P. V. Shekhar, Supramolecular Complex Formation between Rad6 and Proteins of the p53 Pathway during DNA Damage-Induced Response. *Molecular and Cellular Biology* **23**, 2463-2475 (2003).
26. J. Shloush, J. E. Vlassov, I. Engson, S. Duan, V. Saridakis, S. Dhe-paganon, B. Raught, Y. Sheng, C. H. Arrowsmith, Structural and Functional Comparison of the RING Domains of Two p53 E3 Ligases, Mdm2 and Pirh2. *Journal of Biological Chemistry* **286**, 4796-4808 (2011).
27. J. W. VanLandingham, C. A. Fitch, C. W. Levenson, Zinc inhibits the nuclear translocation of the tumor suppressor protein p53 and protects cultured human neurons from copper-induced neurotoxicity. *Neuromolecular medicine* **1**, 171-182 (2002).
28. V. S. Narayanan, C. A. Fitch, C. W. Levenson, Tumor suppressor protein p53 mRNA and subcellular localization are altered by changes in cellular copper in human Hep G2 cells. *The Journal of nutrition* **131**, 1427-1432 (2001).
29. V. M. Phatak, P. A. Muller, Metal toxicity and the p53 protein: an intimate relationship. *Toxicology Research* **4**, 576-591 (2015).
30. S. H. Chen, S. H. Liu, Y.-C. Liang, J.-K. Lin, S.-Y. Lin-Shiau, Death signaling pathway induced by pyrrolidine dithiocarbamate-Cu2+ complex in the cultured rat cortical astrocytes. *Glia* **31**, 249-261 (2000).
31. F. Åslund, M. Zheng, J. Beckwith, G. Storz, Regulation of the OxyR transcription factor by hydrogen peroxide and the cellular thiol—disulfide status. *Proceedings of the National Academy of Sciences* **96**, 6161-6165 (1999).

32. A. Lyakhovich, M. P. Shekhar, Supramolecular complex formation between Rad6 and proteins of the p53 pathway during DNA damage-induced response. *Mol Cell Biol* **23**, 2463-2475 (2003).
33. M. T. Morgan, D. Bourassa, S. Harankhedkar, A. M. McCallum, S. A. Zlatic, J. S. Calvo, G. Meloni, V. Faundez, C. J. Fahrni, Ratiometric two-photon microscopy reveals attomolar copper buffering in normal and Menkes mutant cells. *Proc Natl Acad Sci U S A* **116**, 12167-12172 (2019).
34. Z. Xiao, L. Gottschlich, R. van der Meulen, S. R. Udagedara, A. G. Wedd, Evaluation of quantitative probes for weaker Cu(i) binding sites completes a set of four capable of detecting Cu(i) affinities from nanomolar to attomolar. *Metallomics* **5**, 501-513 (2013).
35. L. Banci, I. Bertini, S. Ciofi-Baffoni, I. Leontari, M. Martinelli, P. Palumaa, R. Sillard, S. Wang, Human Sco1 functional studies and pathological implications of the P174L mutant. *Proc Natl Acad Sci U S A* **104**, 15-20 (2007).
36. K. Houben, C. Dominguez, F. M. van Schaik, H. T. Timmers, A. M. Bonvin, R. Boelens, Solution structure of the ubiquitin-conjugating enzyme UbcH5B. *J Mol Biol* **344**, 513-526 (2004).
37. M. Zimmermann, O. Clarke, J. M. Gulbis, D. W. Keizer, R. S. Jarvis, C. S. Cobbett, M. G. Hinds, Z. Xiao, A. G. Wedd, Metal binding affinities of Arabidopsis zinc and copper transporters: selectivities match the relative, but not the absolute, affinities of their amino-terminal domains. *Biochemistry* **48**, 11640-11654 (2009).
38. A. J. Middleton, J. D. Wright, C. L. Day, Regulation of E2s: A Role for Additional Ubiquitin Binding Sites? *J Mol Biol* **429**, 3430-3440 (2017).
39. P. Y. Wu, M. Hanlon, M. Eddins, C. Tsui, R. S. Rogers, J. P. Jensen, M. J. Matunis, A. M. Weissman, C. Wolberger, C. M. Pickart, A conserved catalytic residue in the ubiquitin-conjugating enzyme family. *EMBO J* **22**, 5241-5250 (2003).
40. K. Nomura, M. Klejnot, D. Kowalczyk, A. K. Hock, G. J. Sibbet, K. H. Vousden, D. T. Huang, Structural analysis of MDM2 RING separates degradation from regulation of p53 transcription activity. *Nat Struct Mol Biol* **24**, 578-587 (2017).
41. E. Sakata, T. Satoh, S. Yamamoto, Y. Yamaguchi, M. Yagi-Utsumi, E. Kurimoto, K. Tanaka, S. Wakatsuki, K. Kato, Crystal structure of UbcH5b~ubiquitin intermediate: insight into the formation of the self-assembled E2~Ub conjugates. *Structure* **18**, 138-147 (2010).
42. C. Michelle, P. Vourc'h, L. Mignon, C. R. Andres, What was the set of ubiquitin and ubiquitin-like conjugating enzymes in the eukaryote common ancestor? *J Mol Evol* **68**, 616-628 (2009).
43. A. Sebe-Pedros, B. M. Degnan, I. Ruiz-Trillo, The origin of Metazoa: a unicellular perspective. *Nat Rev Genet* **18**, 498-512 (2017).
44. H. D. Ryoo, A. Bergmann, H. Gonen, A. Ciechanover, H. Steller, Regulation of Drosophila IAP1 degradation and apoptosis by reaper and ubcD1. *Nat Cell Biol* **4**, 432-438 (2002).
45. T. C. Yeh, S. B. Bratton, Caspase-dependent regulation of the ubiquitin-proteasome system through direct substrate targeting. *Proc Natl Acad Sci U S A* **110**, 14284-14289 (2013).
46. C. T. Kuo, S. Zhu, S. Younger, L. Y. Jan, Y. N. Jan, Identification of E2/E3 ubiquitinating enzymes and caspase activity regulating Drosophila sensory neuron dendrite pruning. *Neuron* **51**, 283-290 (2006).

47. S. Rumpf, J. A. Bagley, K. L. Thompson-Peer, S. Zhu, D. Gorczyca, R. B. Beckstead, L. Y. Jan, Y. N. Jan, Drosophila Valosin-Containing Protein is required for dendrite pruning through a regulatory role in mRNA metabolism. *Proc Natl Acad Sci U S A* **111**, 7331-7336 (2014).
48. C. Pan, Y. Xiong, X. Lv, Y. Xia, S. Zhang, H. Chen, J. Fan, W. Wu, F. Liu, H. Wu, Z. Zhou, L. Zhang, Y. Zhao, UbcD1 regulates Hedgehog signaling by directly modulating Ci ubiquitination and processing. *EMBO Rep* **18**, 1922-1934 (2017).
49. M. Norgate, E. Lee, A. Southon, A. Farlow, P. Batterham, J. Camakaris, R. Burke, Essential roles in development and pigmentation for the Drosophila copper transporter DmATP7. *Mol Biol Cell* **17**, 475-484 (2006).
50. S. W. Mercer, R. Burke, Evidence for a role for the putative Drosophila hGRX1 orthologue in copper homeostasis. *Biometals* **29**, 705-713 (2016).
51. J. E. Hwang, M. de Bruyne, C. G. Warr, R. Burke, Copper overload and deficiency both adversely affect the central nervous system of Drosophila. *Metallomics* **6**, 2223-2229 (2014).
52. T. Binks, J. C. Lye, J. Camakaris, R. Burke, Tissue-specific interplay between copper uptake and efflux in Drosophila. *J Biol Inorg Chem* **15**, 621-628 (2010).
53. S. N. Bocca, M. Muzzopappa, S. Silberstein, P. Wappner, Occurrence of a putative SCF ubiquitin ligase complex in Drosophila. *Biochemical and biophysical research communications* **286**, 357-364 (2001).
54. L. Krishnamoorthy, J. A. Cotruvo Jr, J. Chan, H. Kaluarachchi, A. Muchenditsi, V. S. Pendyala, S. Jia, A. T. Aron, C. M. Ackerman, M. N. V. Wal, T. Guan, L. P. Smaga, S. L. Farhi, E. J. New, S. Lutsenko, C. J. Chang, Copper regulates cyclic-AMP-dependent lipolysis. *Nat Chem Biol* **12**, 586-592 (2016).
55. B. Zhang, T. Binks, R. Burke, The E3 ubiquitin ligase Slimb/β-TrCP is required for normal copper homeostasis in Drosophila. *Biochimica et Biophysica Acta (BBA) - Molecular Cell Research* **1867**, 118768 (2020).
56. X. Chen, X. Zhang, J. Chen, Q. Yang, L. Yang, D. Xu, P. Zhang, X. Wang, J. Liu, Hinokitiol copper complex inhibits proteasomal deubiquitination and induces paraptosis-like cell death in human cancer cells. *European Journal of Pharmacology* **815**, 147-155 (2017).
57. K. J. Waldron, J. C. Rutherford, D. Ford, N. J. Robinson, Metalloproteins and metal sensing. *Nature* **460**, 823-830 (2009).
58. A. D. Anbar, A. H. Knoll, Proterozoic ocean chemistry and evolution: a bioinorganic bridge? *Science* **297**, 1137-1142 (2002).
59. G. Peers, N. M. Price, Copper-containing plastocyanin used for electron transport by an oceanic diatom. *Nature* **441**, 341-344 (2006).
60. V. A. Belyi, P. Ak, E. Markert, H. Wang, W. Hu, A. Puzio-Kuter, A. J. Levine, The origins and evolution of the p53 family of genes. *Cold Spring Harb Perspect Biol* **2**, a001198 (2010).
61. T. Wang, Y. Liu, Y. Fu, T. Huang, Y. Yang, S. Li, C. Li, Antiproliferative activity of di-2-pyridylhydrazone dithiocarbamate acetate partly involved in p53 mediated apoptosis and autophagy. *Int J Oncol* **51**, 1909-1919 (2017).
62. A. Gupte, R. J. Mumper, Elevated copper and oxidative stress in cancer cells as a target for cancer treatment. *Cancer Treatment Reviews* **35**, 32-46 (2009).

63. L. Aubert, N. Nandagopal, Z. Steinhart, G. Lavoie, S. Nourreddine, J. Berman, M. K. Saba-El-Leil, D. Papadopoli, S. Lin, T. Hart, Copper bioavailability is a KRAS-specific vulnerability in colorectal cancer. *Nature communications* **11**, 1-15 (2020).
64. D. Denoyer, S. Masaldan, S. La Fontaine, M. A. Cater, Targeting copper in cancer therapy: 'Copper That Cancer'. *Metallomics* **7**, 1459-1476 (2015).
65. N. Chan, A. Willis, N. Kornhauser, M. M. Ward, S. B. Lee, E. Nackos, B. R. Seo, E. Chuang, T. Cigler, A. Moore, D. Donovan, M. V. Cobham, V. Fitzpatrick, S. Schneider, A. Wiener, J. Guillaume-Abraham, E. Aljom, R. Zelkowitz, J. D. Warren, M. E. Lane, C. Fischbach, V. Mittal, L. Vahdat, Influencing the Tumor Microenvironment: A Phase II Study of Copper Depletion Using Tetrathiomolybdate in Patients with Breast Cancer at High Risk for Recurrence and in Preclinical Models of Lung Metastases. *Clinical cancer research : an official journal of the American Association for Cancer Research* **23**, 666-676 (2017).
66. S. A. James, I. Volitakis, P. A. Adlard, J. A. Duce, C. L. Masters, R. A. Cherny, A. I. Bush, Elevated labile Cu is associated with oxidative pathology in Alzheimer disease. *Free Radic Biol Med* **52**, 298-302 (2012).
67. A. Rembach, J. D. Doecke, B. R. Roberts, A. D. Watt, N. G. Faux, I. Volitakis, K. K. Pertile, R. L. Rumble, B. O. Trounson, C. J. Fowler, W. Wilson, K. A. Ellis, R. N. Martins, C. C. Rowe, V. L. Villemagne, D. Ames, C. L. Masters, AIBL research group, A. I. Bush, Longitudinal analysis of serum copper and ceruloplasmin in Alzheimer's disease. *J Alzheimers Dis* **34**, 171-182 (2013).
68. S. Ayton, P. Lei, J. A. Duce, B. X. Wong, A. Sedjahtera, P. A. Adlard, A. I. Bush, D. I. Finkelstein, Ceruloplasmin dysfunction and therapeutic potential for Parkinson disease. *Ann Neurol* **73**, 554-559 (2013).
69. F. Checler, C. A. da Costa, p53 in neurodegenerative diseases and brain cancers. 1-15 (2014).
70. D. Religa, D. Strozyk, R. A. Cherny, I. Volitakis, V. Haroutunian, B. Winblad, J. Naslund, A. I. Bush, Elevated cortical zinc in Alzheimer disease. *Neurology* **67**, 69-75 (2006).
71. H. Kessler, T. A. Bayer, D. Bach, T. Schneider-Axmann, T. Supprian, W. Herrmann, M. Haber, G. Multhaup, P. Falkai, F.-G. Pajonk, Intake of copper has no effect on cognition in patients with mild Alzheimer's disease: a pilot phase 2 clinical trial. *Journal of Neural Transmission* **115**, 1181-1187 (2008).
72. P. A. Adlard, R. A. Cherny, D. I. Finkelstein, E. Gautier, E. Robb, M. Cortes, I. Volitakis, X. Liu, J. P. Smith, K. Perez, K. Laughton, Q. X. Li, S. A. Charman, J. A. Nicolazzo, S. Wilkins, K. Deleva, T. Lynch, G. Kok, C. W. Ritchie, R. E. Tanzi, R. Cappai, C. L. Masters, K. J. Barnham, A. I. Bush, Rapid restoration of cognition in Alzheimer's transgenic mice with 8-hydroxy quinoline analogs is associated with decreased interstitial Abeta. *Neuron* **59**, 43-55 (2008).
73. C. Opazo, X. Huang, R. A. Cherny, R. D. Moir, A. E. Roher, A. R. White, R. Cappai, C. L. Masters, R. E. Tanzi, N. C. Inestrosa, Metalloenzyme-like activity of Alzheimer's disease β-amyloid Cu-dependent catalytic conversion of dopamine, cholesterol, and biological reducing agents to neurotoxic H2O2. *Journal of Biological Chemistry* **277**, 40302-40308 (2002).
74. O. Nyabi, M. Bentahir, K. Horré, A. Herreman, N. Gottardi-Littell, C. Van Broeckhoven, P. Merchiers, K. Spittaels, W. Annaert, B. De Strooper, Presenilins Mutated at Asp-257

or Asp-385 Restore Pen-2 Expression and Nicastrin Glycosylation but Remain Catalytically Inactive in the Absence of Wild Type Presenilin. *Journal of Biological Chemistry* **278**, 43430-43436 (2003).

75. S. La Fontaine, S. D. Firth, J. Camakaris, A. Englezou, M. B. Theophilos, M. J. Petris, M. Howie, P. J. Lockhart, M. Greenough, H. Brooks, Correction of the copper transport defect of Menkes patient fibroblasts by expression of the Menkes and Wilson ATPases. *Journal of Biological Chemistry* **273**, 31375-31380 (1998).
76. T. Burckstummer, C. Banning, P. Hainzl, R. Schobesberger, C. Kerzendorfer, F. M. Pauler, D. Chen, N. Them, F. Schischlik, M. Rebsamen, M. Smida, F. Fece de la Cruz, A. Lapao, M. Liszt, B. Eizinger, P. M. Guenzl, V. A. Blomen, T. Konopka, B. Gapp, K. Parapatics, B. Maier, J. Stockl, W. Fischl, S. Salic, M. R. Taba Casari, S. Knapp, K. L. Bennett, C. Bock, J. Colinge, R. Kralovics, G. Ammerer, G. Casari, T. R. Brummelkamp, G. Superti-Furga, S. M. Nijman, A reversible gene trap collection empowers haploid genetics in human cells. *Nature methods* **10**, 965-971 (2013).
77. J. W. Zmijewski, S. Banerjee, H. Bae, A. Friggeri, E. R. Lazarowski, E. Abraham, Exposure to hydrogen peroxide induces oxidation and activation of AMP-activated protein kinase. *J Biol Chem* **285**, 33154-33164 (2010).
78. B. Poole, M. Wibo, Protein Degradation in Cultured Cells. The effect of fresh medium, fluoride, and iodoacetate on the digestion of cellular protein of rat fibroblasts. *Journal of Biological Chemistry* **248**, 6221-6226 (1973).
79. F. C. Fiesel, E. L. Moussaud-Lamodiere, M. Ando, W. Springer, A specific subset of E2 ubiquitin-conjugating enzymes regulate Parkin activation and mitophagy differently. *J Cell Sci* **127**, 3488-3504 (2014); published online EpubAug 15 (10.1242/jcs.147520).
80. M. A. Greenough, I. Volitakis, Q.-X. Li, K. Laughton, G. Evin, M. Ho, A. H. Dalziel, J. Camakaris, A. I. Bush, Presenilins promote the cellular uptake of copper and zinc and maintain copper chaperone of SOD1-dependent copper/zinc superoxide dismutase activity. *Journal of Biological Chemistry* **286**, 9776-9786 (2011).
81. S. Tyanova, T. Temu, J. Cox, The MaxQuant computational platform for mass spectrometry-based shotgun proteomics. *Nat. Protocols* **11**, 2301-2319 (2016).
82. D. R. Croucher, M. Iconomou, J. F. Hastings, S. P. Kennedy, J. Z. R. Han, R. F. Shearer, J. McKenna, A. Wan, J. Lau, S. Aparicio, D. N. Saunders, Bimolecular complementation affinity purification (BiCAP) reveals dimer-specific protein interactions for ERBB2 dimers. *Science Signaling* **9**, ra69-ra69 (2016).
83. P. Pagel, S. Kovac, M. Oesterheld, B. Brauner, I. Dunger-Kaltenbach, G. Frishman, C. Montrone, P. Mark, V. Stümpflen, H.-W. Mewes, The MIPS mammalian protein–protein interaction database. *Bioinformatics* **21**, 832-834 (2004).
84. V. G. Tusher, R. Tibshirani, G. Chu, Significance analysis of microarrays applied to the ionizing radiation response. *Proc Natl Acad Sci USA* **98** (2001).
85. D. Szklarczyk, J. H. Morris, H. Cook, M. Kuhn, S. Wyder, M. Simonovic, A. Santos, N. T. Doncheva, A. Roth, P. Bork, L. J. Jensen, C. von Mering, The STRING database in 2017: quality-controlled protein–protein association networks, made broadly accessible. *Nucleic Acids Research* **45**, D362-D368 (2017).
86. Y. Assenov, F. Ramírez, S.-E. Schelhorn, T. Lengauer, M. Albrecht, Computing topological parameters of biological networks. *Bioinformatics* **24**, 282-284 (2008).
87. R. Saito, M. E. Smoot, K. Ono, J. Ruscheinski, P.-L. Wang, S. Lotia, A. R. Pico, G. D. Bader, T. Ideker, A travel guide to Cytoscape plugins. *Nat Meth* **9**, 1069-1076 (2012).

88. J. Yoon, A. Blumer, K. Lee, An algorithm for modularity analysis of directed and weighted biological networks based on edge-betweenness centrality. *Bioinformatics* **22**, 3106-3108 (2006).
89. Y. Sato, A. Yoshikawa, A. Yamagata, H. Mimura, M. Yamashita, K. Ookata, O. Nureki, K. Iwai, M. Komada, S. Fukai, Structural basis for specific cleavage of Lys 63-linked polyubiquitin chains. *Nature* **455**, 358-362 (2008).
90. Z. Xiao, J. Brose, S. Schimo, S. M. Ackland, S. La Fontaine, A. G. Wedd, Unification of the copper(I) binding affinities of the metallo-chaperones Atx1, Atox1 and related proteins: detection probes and affinity standards. *J Biol Chem* **286**, 11047-11055 (2011).
91. M. I. Stefan, N. Le Novère, Cooperative Binding. *PLOS Computational Biology* **9**, e1003106 (2013).
92. S. G. Hyberts, K. Takeuchi, G. Wagner, Poisson-Gap Sampling and Forward Maximum Entropy Reconstruction for Enhancing the Resolution and Sensitivity of Protein NMR Data. *Journal of the American Chemical Society* **132**, 2145-2147 (2010).
93. F. Delaglio, S. Grzesiek, G. W. Vuister, G. Zhu, J. Pfeifer, A. Bax, NMRPipe: A multidimensional spectral processing system based on UNIX pipes. *Journal of Biomolecular NMR* **6**, 277-293 (1995).
94. J. Ying, F. Delaglio, D. A. Torchia, A. Bax, Sparse multidimensional iterative lineshape-enhanced (SMILE) reconstruction of both non-uniformly sampled and conventional NMR data. *Journal of Biomolecular NMR* **68**, 101-118 (2017).
95. S. A. Lee, S. M. Kim, B. K. Suh, H. Y. Sun, Y. U. Park, J. H. Hong, C. Park, M. D. Nguyen, K. Nagata, J. Y. Yoo, S. K. Park, Disrupted-in-schizophrenia 1 (DISC1) regulates dysbindin function by enhancing its stability. *J Biol Chem* **290**, 7087-7096 (2015).
96. A. Ayed, F. A. A. Mulder, G.-S. Yi, Y. Lu, L. E. Kay, C. H. Arrowsmith, Latent and active p53 are identical in conformation. *Nature Structural Biology* **8**, 756-760 (2001).
97. C. Camacho, G. Coulouris, V. Avagyan, N. Ma, J. Papadopoulos, K. Bealer, T. L. Madden, BLAST+: architecture and applications. *BMC Bioinformatics* **10**, 421 (2009).
98. R. Desper, O. Gascuel, Theoretical foundation of the balanced minimum evolution method of phylogenetic inference and its relationship to weighted least-squares tree fitting. *Mol Biol Evol* **21**, 587-598 (2004).
99. N. V. Grishin, Estimation of the number of amino acid substitutions per site when the substitution rate varies among sites. *J Mol Evol* **41**, 675-679 (1995).
100. Y. Zhou, B. Zhou, L. Pache, M. Chang, A. H. Khodabakhshi, O. Tanaseichuk, C. Benner, S. K. Chanda, Metascape provides a biologist-oriented resource for the analysis of systems-level datasets. *Nat Commun* **10**, 1523 (2019).
101. K. Baek, D. T. Krist, J. R. Prabu, S. Hill, M. Klügel, L.-M. Neumaier, S. von Gronau, G. Kleiger, B. A. Schulman, NEDD8 nucleates a multivalent cullin–RING–UBE2D ubiquitin ligation assembly. *Nature* **578**, 461-466 (2020).
102. N. King, M. J. Westbrook, S. L. Young, A. Kuo, M. Abedin, J. Chapman, S. Fairclough, U. Hellsten, Y. Isogai, I. Letunic, M. Marr, D. Pincus, N. Putnam, A. Rokas, K. J. Wright, R. Zuzow, W. Dirks, M. Good, D. Goodstein, D. Lemons, W. Li, J. B. Lyons, A. Morris, S. Nichols, D. J. Richter, A. Salamov, J. G. Sequencing, P. Bork, W. A. Lim, G. Manning, W. T. Miller, W. McGinnis, H. Shapiro, R. Tjian, I. V. Grigoriev, D. Rokhsar, The genome of the choanoflagellate Monosiga brevicollis and the origin of metazoans. *Nature* **451**, 783-788 (2008).

Acknowledgements

We thank A. Ciechanover (Technion-Israel Institute of Technology, Israel), G. Schwarz (University of Cologne, Germany), B. J. Monahan and D. Komander (Walter and Eliza Hall Institute of Medical Research, Australia), J. Camakaris, B. Dean, G. Pavey, R. A. Cherny, S. Luza, I. Volitakis, V. Perreau, A. Southon, A. Lothian, B. Turner and K. Dent (The Florey Institute of Neuroscience and Mental Health, Australia), A.G. Wedd and Shenggen Yao (Bio21 Institute, The University of Melbourne, Australia), S. Lutsenko (Johns Hopkins University), Chris Chang (Berkeley University), L.G. Aguayo, C. López, L. Guzmán, G. Moraga-Cid, M. Reyes (University of Concepción, Chile), C. Peters (Max Planck Institute of Neurobiology, Germany), C. Aylwin, (Oregon Health and Sciences University, USA), M. A. Cater (Deakin University, Australia), M. Avila (Universidad de las Américas, Chile), G. De Ferrari (Universidad Andrés Bello, Chile), B. Roberts (Emory University, USA), N. Faux (IBM Research-Australia), M. Cortés and E.L. Robb (Mental Health Research Institute of Victoria, Australia).

Funding: The Florey Institute of Neuroscience and Mental Health acknowledges the strong support from the Victorian Government and in particular the funding from the Operational Infrastructure Support Grant. This work was supported by the Australian Research Council (AIB, ZX and CO), the National Health and Medical Research Council (AIB, DNS), and the CRC for Mental Health (AIB); grant ACT-04 from the Chilean Government (CO); as well as MNDRIA, Guest Family (DNS). We are grateful for the AUSiMED Fellowship Grant (AL) made possible by the generosity of the Lowy Foundation.

Author contributions: H.T. M.A.G. and C.M.O, performed the Western blot analyses. A.A.U. and Z.X. prepared the plasmids, expressed and purified the E2D2 proteins, performed the mutation analysis on E2D2 and the copper binding studies. J.M. collected MS ubiquitomics data. D.N.S. and A.L. analyzed the ubiquitome data. M.A.G. performed the AMS binding assay, proteasome activity assay and co-immunoprecipitation experiments. C.M.O, C.M.L. and H.T. performed the *in vitro* ubiquitin conjugation assays. C.M.O., C.M.L. and C.H.M. performed the protein pulse-chase experiments. Z.X. designed the structural analyses. A.R. and C.M.O performed the studies with siRNAs. A.L. performed the sequence, evolution and statistical analyses. R.B., C.M.O., Z.X. and A.I.B. discussed the *Drosophila* studies. R.B. designed, evaluated and interpreted the

Drosophila data. B.Z. performed the *Drosophila* studies. P.G. and Z.X. designed and performed the NMR studies and P.R.G., Z.X and A.I.B. discussed the NMR data; A.L., C.M.O, Z.X., R.B., D.N.S, P.R.G and A.I.B. wrote the manuscript. All authors read and approved the final manuscript

Competing financial interests: Prof. Bush is a shareholder in Alterity Therapeutics Ltd, Cogstate Ltd, Brighton Biotech LLC, Grunbiotics Pty Ltd, Eucalyptus Pty Ltd, and Mesoblast Ltd. He is a paid consultant for, and has a profit share interest in, Collaborative Medicinal Development Pty Ltd.

Data and materials availability: All data is available in the manuscript or the supplementary materials

Supplementary Materials:

Materials and Methods

Supplementary Text

Figures S1-S11

Tables S1-S4

Data S1-S8

References (*73-100*)